LINEAR UNIVERSAL DEMOSAICKING OF REGULAR PATTERN COLOR FILTER ARRAYS

Mritunjay Singh

Image Algorithmics
msingh@imagealgorithmics.com

Tripurari Singh

Image Algorithmics
tsingh@imagealgorithmics.com

ABSTRACT

We show that a recently developed universal demosaicker by the present authors greatly outperforms existing demosaickers when tested with a realistic optical pipeline. We present speed and quality optimizations of this demosaicker for the case of regular pattern color filter arrays.

We implement and extensively test optimized versions for several common CFAs including Bayer, CMY and several RGBW patterns. These tests show that the proposed algorithms outperform other demosaickers by a substantial margin while being faster than most of them. High sensitivity RGBW CFAs are shown to have better performance than Bayer demosaicked with previous algorithms.

The proposed universal demosaicker is a set of Finite Impulse Response Filters, which allows a single, efficient, Image Signal Processor design to support different CFAs by changing its filter weights. Being linear, the demosaicker is free of noise induced artifacts and outputs images with near Poissonian noise which is noise reduction friendly.

Index Terms— Universal, Demosaicking, Bayer, RGBW

1. INTRODUCTION

A universal demosaicker was first introduced in [1] wherein a constant color ratio model in conjunction with a numerical stabilization technique was used to interpolate missing pixel values in primary color CFAs. Subsequently [2] introduced a variation minimization based demosaicker that was not restricted to primary color CFAs and out-performed [1] on certain random CFAs. Neither of these universal demosaickers, however, could match the performance of leading Bayer-specific algorithms on the Bayer CFA such as [3], [4], [5] and [6].

More recently [7] introduced an universal demosaicker for limited luminance and chrominance bandwidth models that reduced the demosaicking problem to solving a system of linear equations. When applied to random RGB CFAs with luminance and chrominance bandwidths typically found in commercial systems, this algorithm out-performed existing Bayer systems.

In this paper, we present an optimization of [7] for the case of simple repeating pattern CFAs. Such patterns are comprised of a small number of carriers. A frequency domain formulation of the demosaicking problem is shown to be sparse and decomposable leading to better run time performance.

Patent Pending

2. FORMULATION OF THE DEMOSAICKING PROBLEM

Consider a discrete image with (N_1, N_2) pixels. Denote the R, G, B color planes of the image by $\boldsymbol{x}_i, i \in \{r, g, b\}$ and those of the CFA that filters it by $\boldsymbol{c}_i, i \in \{r, g, b\}$. Now, a photosite located at $\boldsymbol{n} = (n_1, n_2), 1 \leq n_1 \leq N_1, 1 \leq n_2 \leq N_2$ filters the incident light $\boldsymbol{x}(\boldsymbol{n}) = \begin{bmatrix} x_r(\boldsymbol{n}) & x_g(\boldsymbol{n}) & x_b(\boldsymbol{n}) \end{bmatrix}^T$ through color filter array $\boldsymbol{c}(\boldsymbol{n}) = \begin{bmatrix} c_r(\boldsymbol{n}) & c_g(\boldsymbol{n}) & c_b(\boldsymbol{n}) \end{bmatrix}$ and measures the resulting noise-free, scalar signal $y(\boldsymbol{n})$, where

$$y(\boldsymbol{n}) = \boldsymbol{c}(\boldsymbol{n}) \cdot \boldsymbol{x}(\boldsymbol{n}) \tag{1}$$

Following the frequency domain formulation of [7], taking (N_1, N_2) point 2D DFT of both sides we have,

$$\boldsymbol{Y} = \sum_{i \in \{r,g,b\}} \boldsymbol{C}_i * \boldsymbol{X}_i \tag{2}$$

where $\boldsymbol{Y}$, $\boldsymbol{C}_i$, $\boldsymbol{X}_i, i \in \{r, g, b\}$ are the 2D DFT of y, $\boldsymbol{c}_i$, $x_i, i \in \{r, g, b\}$ respectively and $*$ represents 2D convolution. The non-zero elements of $\boldsymbol{C}_i$ correspond to modulation carriers. In order to cast Equation 2 in matrix form, we first define $\tilde{\boldsymbol{Y}}, \tilde{\boldsymbol{X}}_i, \tilde{\boldsymbol{C}}_i, i \in \{r, g, b\}$ as the row-major column vector versions of $\boldsymbol{Y}, \boldsymbol{X}_i, \boldsymbol{C}_i, i \in \{r, g, b\}$ respectively and $\tilde{\boldsymbol{X}} \equiv \begin{bmatrix} \tilde{\boldsymbol{X}}_r & \tilde{\boldsymbol{X}}_g & \tilde{\boldsymbol{X}}_b \end{bmatrix}^T$ as the concatenation of $\tilde{\boldsymbol{X}}_r, \tilde{\boldsymbol{X}}_g, \tilde{\boldsymbol{X}}_b$. Furthermore, denote DFT frequencies of the input image by $\boldsymbol{\omega} = (\omega_1, \omega_2)$ and those of the CFA filtered image by $\boldsymbol{\Omega} = (\Omega_1, \Omega_2)$ and their row-major column vector versions as $\tilde{\omega}$ and $\tilde{\Omega}$ respectively. Now Equation 2 can be re-written in matrix form as

$$\tilde{\boldsymbol{Y}} = \boldsymbol{A} \cdot \tilde{\boldsymbol{X}} \tag{3}$$

where row $\tilde{\Omega}$ of A is the concatenation of $\tilde{\boldsymbol{D}}_i(\tilde{\Omega}), i \in \{r, g, b\}$,

$$\boldsymbol{A}(\tilde{\Omega}) \equiv \begin{bmatrix} \tilde{\boldsymbol{D}}_r(\tilde{\Omega}) & \tilde{\boldsymbol{D}}_g(\tilde{\Omega}) & \tilde{\boldsymbol{D}}_b(\tilde{\Omega}) \end{bmatrix} \tag{4}$$

and $\tilde{\boldsymbol{D}}_i(\tilde{\Omega}), i \in \{r, g, b\}$ is a row vector obtained by appropriately rearranging the elements of $\tilde{\boldsymbol{C}}_i^T, i \in \{r, g, b\}$ so as to effect the convolution of Equation 2.

This system of linear equations can be solved to determine $\tilde{\boldsymbol{X}}$ if the rank of $\boldsymbol{A}$ is no less than $|\tilde{\boldsymbol{X}}|$, where $|.|$ denotes cardinality. Since the rank of matrix $\boldsymbol{A}$ cannot exceed $|\tilde{\boldsymbol{Y}}|$ which itself is one third of the cardinality of $\tilde{\boldsymbol{X}}$ for the case of three basic colors, additional constraints are required to meet the above condition. We choose the constraints that the signal is bandlimited, and has low chrominance bandwidth so that two thirds or more elements of $\tilde{\boldsymbol{X}}$ may be taken to be zero. We obtain $\tilde{\boldsymbol{X}}'$ from $\tilde{\boldsymbol{X}}$ by moving to a luminance/chrominance color space and dropping elements of $\tilde{\boldsymbol{X}}$ corresponding to the above constraints. $\boldsymbol{A}'$ is obtained by making the corresponding changes to $\boldsymbol{A}$. This gives

$$\tilde{\boldsymbol{Y}} = \boldsymbol{A}' \cdot \tilde{\boldsymbol{X}}' \tag{5}$$

which leads to the solution

$$\tilde{\boldsymbol{X}}' = \boldsymbol{A}'^{-1} \cdot \tilde{\boldsymbol{Y}} \tag{6}$$

where $\boldsymbol{A}'^{-1}$ is a generalized inverse of $\boldsymbol{A}'$.

It should be noted that any transform with good energy compaction properties can be substituted for the DFT in the above analysis, as long as care is taken with the Convolution Theorem.

3. OPTIMIZATIONS FOR CFAS WITH FEW CARRIERS

For CFAs composed of a small number of carriers, each DFT coefficient of the CFA filtered image is connected to only a small number of other DFT coefficients by the equations 5. The transformation matrix, $\boldsymbol{S}$, becomes sparse and decomposable and DFT coefficients of the input image can therefore be computed using generalized inverses of small matrices. Additionally, sets of sub-domains of the input image frequency space may be identified such each set requires the computation of the generalized inverse of identical matrices.

We consider the problem of constructing the sets mentioned above, illustrating the construction with the Bayer CFA as an example. The Bayer CFA has just three carriers as shown in Figure 1(a). The relevant color components are the luminance L and chrominances C1 and C2 as defined in [4]. For the present example, luminance resolution is set to 0.83 of the Nyquist limit and chrominance resolution is set to half of luminance resolution.

The bandlimitedness conditions on the color components of the input image define their domains Δ_i, typically discs in frequency space.

$$\Delta_i = \{\omega \ : \ \exists \ \tilde{\boldsymbol{X}}'_i(\tilde{\omega})\} \tag{7}$$

where $i \in \{l, c1, c2, \ldots\}$

After modulation by the CFA, these domains get shifted by the carrier frequencies $\omega_c$of the CFA.

$$\Delta_i^{\omega_c} = \{\omega \ : \ \omega = \omega_c + \omega', \ \ \omega' \in \Delta_i\} \tag{8}$$

where ω_c corresponds to non-zero elements of $\boldsymbol{C}_i$.

These shifted domains may overlap, creating boundaries. See Figure 1(a) as an example. The domain boundaries enclose regions in the frequency space of the CFA filtered image.

The following geometrical steps are used to construct the sets:

- For each color component, shift all domain copies back to the baseband, along with domain overlap boundaries lying therein. The union of all domain boundaries of all domain copies may subdivide the domains into smaller sub-domains.
- Repeat the above steps of shifting domain copies, including their divisions, to all carrier frequencies and then shift them back to the baseband till this process results in no new sub-domain formation. In the Bayer example, Figure 1(c) and 1(d) illustrate numbered sub-domains formed in the C2 and L color component domains respectively. The C1 domain forms a single sub-domain by itself. Let these sub-domains be denoted by $\Delta_{i,p}$ where p is the sub-domain number. Let the shifted sub-domains be denoted by $\Delta_{i,p}^{\omega_c}$ where ω_c is the shift frequency.
- Repeat the above step of shifting copies of domains, including their divisions, to all the carrier frequencies one last time. In the Bayer example, this results in the map shown in Figure 1(b). For each bounded region s in this map , we define the set of all overlapping modulated sub-domains in that region:

$$\boldsymbol{O}_s = \{\Delta_{i,p}^{\omega_c} \ : \ \Delta_{i,p}^{\omega_c} \in s\} \tag{9}$$

- Group the resulting sub-domains into sets so that each set $\boldsymbol{T}_q$ contains all domains that either overlap with each or are connected by a chain of overlaps:

$$\begin{aligned}\boldsymbol{T}_q = \{&\Delta_{i,p} \ : \ \forall \ \Delta_{ia,pa}, \Delta_{ib,pb} \ \in \ \boldsymbol{T}_q, \ \exists \ \omega_{ca}, \omega_{cb}, \boldsymbol{O}_{sj}, \\ &\Delta_{il,pl}, \omega_{cl}, \bar{\omega_{cl}}, j = 1 \ldots k, l = 1 \ldots k-1 \ k \geq 0 \ s.t. \\ &\Delta_{ia,pa}^{\omega_{ca}} \in \boldsymbol{O}_{s1}, \ \Delta_{il,pl}^{\omega_{cl}} \in \boldsymbol{O}_{sl}, \\ &\Delta_{il,pl}^{\omega_{cl}} \in \boldsymbol{O}_{s(l+1)}, \ \Delta_{ib,pb}^{\omega_{cb}} \in \boldsymbol{O}_{sk}\}\end{aligned} \tag{10}$$

- Group sets into families of sets $\mathscr{T}_r$ such that all sets in a family result from overlap of the same domain copies.

$$\begin{aligned}\mathscr{T}_r = \{&\boldsymbol{T}_q \ : \ \forall \ \boldsymbol{T}_{q1}, \boldsymbol{T}_{q2} \ \in \ \mathscr{T}_r \ , \exists \ a \ bijection \ f_{q1,q2} \\ &\boldsymbol{T}_{q1} \leftrightarrow \boldsymbol{T}_{q2} \ s.t. \ \forall \ \boldsymbol{O}_{s1} \ s.t. \ \exists \ \Delta_{i,p} \in \ \boldsymbol{O}_{s1}, \exists \ \boldsymbol{O}_{s2} \\ &s.t. \ \forall \ \Delta_{i,q} \in \ \boldsymbol{O}_{s1}, f_{q1,q2}(\Delta_{i,q}) \in \boldsymbol{O}_{s2}\}\end{aligned} \tag{11}$$

The following families of sets definitions result from the above construction procedure.

$$\begin{aligned}\mathscr{T}_1 =& \{\{C1\}\} \\ \mathscr{T}_2 =& \{\{13L\}\} \\ \mathscr{T}_3 =& \{\{9L, 5C2\}, \{10L, 6C2\}\} \\ \mathscr{T}_4 =& \{\{12L, 7C2\}, \{11L, 8C2\}\} \\ \mathscr{T}_5 =& \{\{6L, 2C2, 2L\}, \{5L, 1C2, 1C2\}, \{8L, 4C2, 4L\}, \\ & \{7L, 3C2, 3L\}\}\end{aligned}$$

The following properties hold for the sets and their families so defined:

- All sub-domains in a set are identically shaped. We shall refer to the common shape of all sub-domains belonging to a set as the set template.
- Equations involving any frequency variable from one sub-domain may only involve the corresponding frequency variable from other sub-domains in the same set.
- Similar reduced sets of equations of the form

$$\tilde{\boldsymbol{Y}}_r = \boldsymbol{A}_r \cdot \tilde{\boldsymbol{X}}_r \tag{12}$$

exist for each frequency in the template of each set in a family with each set of equations containing the same transformation matrix $\boldsymbol{A}_r$. Equation 12 is obtained from Equation 5 by selecting only certain columns and rows of $\boldsymbol{A}'$. First, to select columns, a single frequency ω is arbitrarily selected from the template; then $\tilde{\boldsymbol{X}}_r$ is constructed from $\tilde{\boldsymbol{X}}'$ by keeping only the elements corresponding to this frequency ω from each sub-domain which is a member of the set, and discarding the rest. $\boldsymbol{A}_r$ is constructed from $\boldsymbol{A}'$ by keeping only the columns corresponding to the elements of $\tilde{\boldsymbol{X}}_r$. Next, to select rows, we first identify all elements $\boldsymbol{O}_s$ which contain sub-domains from the set in consideration. For each of these elements $\boldsymbol{O}_s$, we keep only the row from $\boldsymbol{A}'$ corresponding to the frequency ω, in $\boldsymbol{A}_r$. We also keep only these rows from $\tilde{\boldsymbol{Y}}$ in $\tilde{\boldsymbol{Y}}_r$.

From the above we conclude that for each family of sets, equations for only a single discrete frequency in a single template need be solved. The pseudo inverse of the transform $\boldsymbol{A}_r$ may be applied to compute all discrete frequencies of the templates of all sets in the family of sets.

The optimized solution has a significant speed advantage both in computing the generalized inverse and in applying it to a particular

image. The above optimized solution has the following additional advantages: this solution gives convenient controls over the solution in the presence of over-determinedness and under-determinedness. In the Bayer example, sub-domains 1,2,3 and 4 in Chrominance C2 may be under-determined and the optimized solution gives easy controls on the treatment of the solution to these sub-domains. For example, we could decide to set these sub-domains to zero.

4. DEMOSAICKING BAYER CFA IMAGES

For the Bayer CFA, the solution resulting from the sets constructed in the previous section may be further reduced to the following.

- Chrominance C1 does not overlap with the other color components if luminance resolution is less than 0.94 times the Nyquist limit and chrominance resolution is half or less of luminance resolution. Therefore C1 may be extracted by demodulation and filtration.
- Chrominance C2 overlaps with luminance if luminance resolution is more than $\frac{2}{3}$ times the Nyquist limit and chrominance resolution is half or more of luminance. C2 has to be pieced together with sections of its two copies, C2a and C2b, that do not overlap with luminance. This may result in some domains of C2 being recoverable from both C2a and from C2b, such as the central domain in depicted in the right column of Figure 2, allowing us to compute its MLE. There may be some domains of C2 that are unrecoverable, such as domains 1,2,3 and 4 in Figure 1(c). Such sub-domains exist if luminance resolution is more than 0.776 times the Nyquist limit and chrominance resolution is half or more of luminance.
- Once C2, or recoverable sub-domains of it, has been recovered, luminance may be extracted by re-modulating C1 and C2 as per the Bayer CFA and subtracting it from the mosaicked image.
- Having reconstructed, C1, C2 and L, a color transform followed by an inverse Fourier transform yields the output RGB image.

The above solution has similarities with [4], except for luminance and chrominance resolutions that are broadly in line with those used by commercial systems and fine tuned to their optics.

A DSLR imaging pipeline was simulated consisting of a lens model, a birefringent OLPF, box filtration due to 100% photosite fill factor, CFA filtration and demosaicking. A F# range of F4-F8 was chosen so as to trade-off spherical aberration and diffraction for the highest resolution image. At F8 diffraction dominated spherical aberration, allowing us simplify the lens model by discarding the latter. Greater than Nyquist resolution was used in order to capture aliasing due to high frequency leakage. A similar exercise was carried out for compact cameras, except the OLPF was omitted. Reconstructed images were compared, in terms of CPSNR, with the input image put through the same imaging pipeline except for the mosaicing-demosaicking step.

Parameter	Compact	DSLR
Lens airy disc diameter	4 pixels	2.2 pixels
Birefringent OLPF shift	none	1 pixel
Box filtering fill factor	100%	100%
Undersampling factor	1x	1.5x

Table 1. Imaging pipeline simulation parameters.

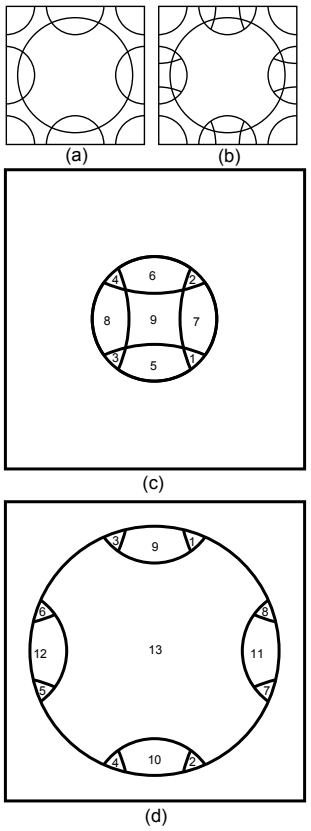

Fig. 1. Bayer sub-domains

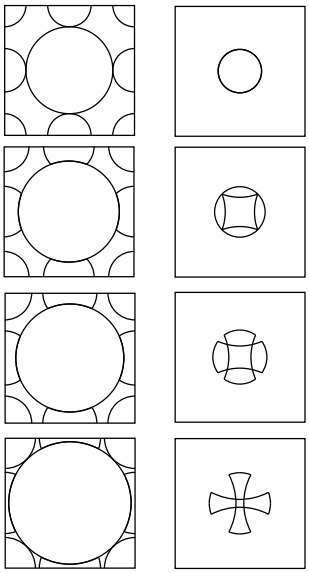

Fig. 2. Spectrum of Bayer filtered image (left column) and recoverable chrominance sub-domains (right column) for several values of luminance resolution: from top to bottom: 0.67, 0.76, 0.83, 0.94 times the Nyquist limit and half chrominance resolution

The proposed demosaicking algorithm, both in the general form (Prop) and in the optimized form (Prop Opt) were compared to two state of the art non-linear demosaickers for the Bayer CFA: LMMSE [6], AHD [5] and POCS [3]. The proposed demosaicking algorithm was tuned to reconstruct luminance at a resolution of 87.7% of the Nyquist limit and chrominance at 51.4% of the luminance resolution, which is competitive with commercial systems. All other demosaicker outputs were post filtered to the same resolutions which marginally improved their CPSNRs. Images from both the Kodak set and the newer IMAX set were used. Results are shown in Table 2.

Image set	Prop	Prop Opt	LMMSE	AHD	POCS
IMAX	46.5	45.2	41.0	39.5	39.6
Kodak	51.7	50.0	47.8	46.1	46.9

Image set	Prop	Prop Opt.	LMMSE	AHD	POCS
IMAX	43.0	41.6	38.5	37.1	37.1
Kodak	48.2	46.2	44.7	43.1	43.4

Table 2. CPSNR (dB) of demosaicking algorithms on the Bayer CFA for the Compact (top) and DSLR (bottom) cameras.

The proposed demosaicker was also tested on the higher sensitivity Bayer CMY CFA, requiring only a change in the color transform used in its final step to handle the CMY variant. Results are shown in Table 4.

Prop Opt	LMMSE	AHD	Bilinear
0.34	24.8	34.3	0.13

Table 3. Run time, in seconds, of MATLAB demosaicker implementations on 512x512 pixel image. Optimized C and DSP implementations are expected to perform very differently.

Image set	Compact	DSLR
IMAX	45.6	41.9
Kodak	50.4	45.5

Table 4. CPSNR (dB) of the proposed demosaicking algorithm on the Bayer CMY CFA for the Compact and DSLR cameras.

5. DEMOSAICKING RGBW CFA IMAGES

Color Filter Arrays (CFA) containing white or panchromatic pixels in addition to RGB have been suggested by Kodak [8], Sony [9] and others [10] as a means of improving luminance sensitivity. All RGBW CFAs suggested so far are regular repeating patterns.

Most existing demosaickers, such as [8], consist of two basic steps: first independently reconstruct a high resolution panchromatic image followed by low resolution chrominance images, then merge these images and output the result.

An empirical comparison of three RGBW patterns, shown in Figure 3 was made using the proposed universal demosaicker, tuned to extract 80% luminance and 50% chrominance resolutions, and the universal demosaicker of Condat [2], whose outputs were post-filtered to the same resolutions marginally improving its CPSNR. Results are shown in Table 5.

Images	Kodak		Sony		Wang et al.	
	Prop	Condat	Prop	Condat	Prop	Condat
IMAX	43.7	38.4	44.7	38.8	46.0	40.2
Kodak	49.1	41.9	48.8	42.4	51.5	43.0

Images	Kodak		Sony		Wang et al.	
	Prop	Condat	Prop	Condat	Prop	Condat
IMAX	40.4	36.0	41.3	36.3	42.5	37.6
Kodak	45.2	39.7	45.2	40.1	47.4	40.7

Table 5. CPSNR (dB) of the proposed universal demosaicker and of Condat's universal demosaicker [2] on Kodak, Sony and Wang RGBW CFAs for the Compact (top) and DSLR (bottom) cameras.

6. CONCLUSION

We optimize a recently developed universal demosaicker for the case of simple repeating pattern CFAs and test it on a number of common CFAs. The proposed demosaicker greatly outperforms existing demosaickers in reconstruction quality while being faster than most. Demosaicking performance of high sensitivity RGBW CFAs is shown to be superior to Bayer with previous demosaickers even in the absence of noise.

The proposed universal demosaicker performs very well in practical settings, producing few artifacts and high CPSNR. Its linearity translates into freedom from directional artifacts, even with high sensor noise, and separable noise reduction. Furthermore, its simplicity and universality enables a single Image Signal Processor (ISP) design that can be programmed to demosaick most CFA patterns, thereby overcoming a significant financial impediment to the adoption of novel CFA designs.

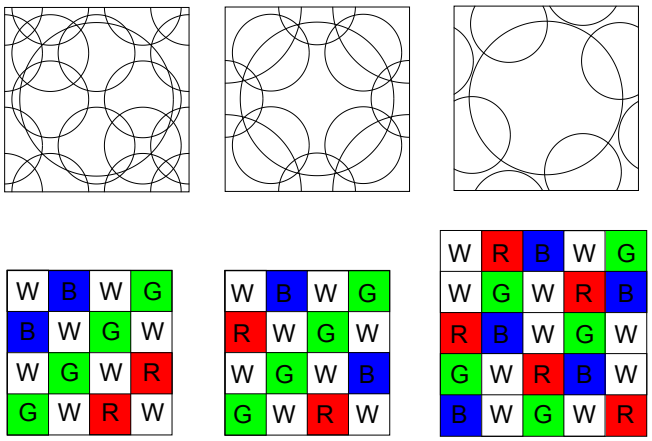

Fig. 3. RGBW CFAs by Kodak, Sony and Wang et al. (left to right) and their spectra.

7. REFERENCES

[1] R. Lukac and K.N. Plataniotis, "Universal demosaicking for imaging pipelines with an RGB color filter array," *Pattern Recognition*, vol. 38, no. 11, pp. 2208–2212, 2005.

[2] L. Condat, "A generic variational approach for demosaicking from an arbitrary color filter array," in *Proc. of IEEE ICIP*, 2009.

[3] Bahadir K. Gunturk, Yucel Altunbasak, and Russell M. Mersereau, "Color plane interpolation using alternating projections," *IEEE Trans. on Image Processing*, vol. 11, pp. 997–1013, 2002.

[4] E. Dubois, "Frequency-domain methods for demosaicking of bayer-sampled color images," *IEEE Signal Processing Letters*, vol. 12, no. 12, pp. 847–850, 2005.

[5] K. Hirakawa and T.W. Parks, "Adaptive homogeneity-directed demosaicing algorithm," *IEEE Trans. on Image Processing*, vol. 14, no. 3, pp. 360–369, 2005.

[6] L. Zhang and X. Wu, "Color demosaicking via directional linear minimum mean square-error estimation," *IEEE Trans. on Image Processing*, vol. 14, no. 12, pp. 2167–2178, 2005.

[7] T. Singh and M. Singh, "Disregarding Spectral Overlap - a unified approach for Demosaicking, Compressive Sensing and Color Filter Array Design," in *Proc. of IEEE ICIP*, 2011.

[8] M. Kumar, E.O. Morales, J.E. Adams, and W. Hao, "New digital camera sensor architecture for low light imaging," in *Proc. of IEEE ICIP*, 2009, pp. 2681–2684.

[9] I. Hirota, "Solid-state imaging device, method for processing signal of solid-state imaging device, and imaging apparatus," Dec. 4 2009, US Patent App. 12/630,988.

[10] J. Wang, C. Zhang, and P. Hao, "New Color Filter Arrays of High Light Sensitivity and High Demosaicking Performance," in *Proc. of IEEE ICIP*, 2011.